

The Classical Hall Effect in Multiply-Connected Plane Regions Part I: Topologies with Stream Function

Udo Ausserlechner

Department of Sense and Control, Infineon Technologies AG, Villach, Austria

Email: udo.ausserlechner@infineon.com

How to cite this paper: Ausserlechner, U. (2019) The Classical Hall Effect in Multiply-Connected Plane Regions Part I: Topologies with Stream Function. *Journal of Applied Mathematics and Physics*, 7, 1968-1996.
<https://doi.org/10.4236/jamp.2019.79136>

Received: July 16, 2019

Accepted: September 6, 2019

Published: September 9, 2019

Copyright © 2019 by author(s) and Scientific Research Publishing Inc.

This work is licensed under the Creative Commons Attribution International License (CC BY 4.0).

<http://creativecommons.org/licenses/by/4.0/>



Open Access

Abstract

Typical Hall plates for practical magnetic field sensing purposes are plane, simply-connected regions with peripheral contacts. Their output voltage is the sum of even and odd functions of the applied magnetic field. They are commonly called offset and Hall voltage. Contemporary smart Hall sensor circuits extract the Hall voltage via spinning current Hall probe schemes, thereby cancelling out the offset very efficiently. The magnetic field response of such Hall plates can be computed via the electric potential or via the stream function. Conversely, Hall plates with holes show new phenomena: 1) the stream function exists only for a limited class of multiply-connected domains, and 2) a sub-class of 1) behaves like a Hall/Anti-Hall bar configuration, *i.e.*, no Hall voltage appears between any two points on the hole boundary if current contacts are on their outer boundary. The paper studies the requirements under which these effects occur. Canonical cases of simply and doubly connected domains are computed analytically. The focus is on 2D multiply-connected Hall plates where all boundaries are insulating and where all current contacts are point sized.

Keywords

Anti-Hall Bar, Doubly Connected, Geometry Factor, Hall Plate, Multiply Connected, Non-Peripheral Contacts, Reverse Magnetic Field Reciprocity, Stream Function

1. Introduction

Conventional Hall plates have no holes. They are well understood, though the analytical calculation of the Hall output voltage remains challenging, particularly

at large magnetic field [1] [2], for contacts of finite size [3], and in the absence of symmetries [4]. There are also several formulae for devices with small output contacts at weak magnetic field [5] [6] [7] [8]. An early mention of bounded Hall plates with a single hole is [9], where the author computed the impedance matrix of symmetric circular rings with large symmetric contacts with the method of conformal mapping. This was a by-product of a calculation of the power delivered by an infinitely long magneto-hydrodynamic generator. It was also proven in a strict mathematical way that these devices give no Hall voltage on the inner sense contacts placed on the x-axis when current is sent through outer supply contacts centered on the y-axis. However, the author did not elaborate on the question, if this effect is due to symmetry only. Moreover it was proven that there is no Hall voltage between any contacts in any symmetric or asymmetric multiply connected conductive region if all its boundaries are conducting—we will pick up this thread in a follow-up paper part II. The Hall effect in double boundary geometries with small contacts was studied in [10] with the goal of reducing the zero point error (offset) of Hall plates. The authors called their rectangular ring “anti-Hall bar within a Hall bar” (see [Figure 1](#)) and focused on the fact that current flowing through points on the outer boundary gives no Hall signal on the inner boundary, and vice versa, whereas the offsets measured on both boundaries are affected by both currents. Multiply-connected Hall-plates with contacts of arbitrary size on the boundaries of holes are investigated in [11] on an advanced mathematical level. Another aspect of Hall plates with ring topology is the reversal of the Hall voltage when sense and supply contacts are on the inner boundaries in contrast to being on the outer boundaries. If a material consists of a huge number of such rings the sign of the macroscopic Hall constant depends on the electrical coupling of the rings. This was predicted theoretically in [12] and verified experimentally in [13]. The funny result is that seemingly in contrast to introductory text books the sign of the Hall voltage does not correctly reveal the sign of the majority charge carriers, unless one takes into account the exact complicated topology of such chainmail-like meta-materials. The same effect was observed in finite-element analyses of van der Pauw-Hall measurements on samples with inhomogeneities [14].

Discontinuous Hall effect regions exhibit similar phenomena as multiply connected Hall Effect regions [15].

This paper gives a theory on the classical Hall effect in multiply-connected plane and schlicht regions bounded by Jordan curves [16]. It may be simple for mathematicians, but engineers and physicists might not be so fluent with this topic. Many building blocks of the theory are well known but dispersed in different fields of engineering sciences such as electromagnetic field theory, conformal mapping theory, and Hall effect theory. Several conclusions are made and rules are derived, which the author has not found published elsewhere. Therefore it seems justified to compile all this in the current paper and present it in an easily accessible way.

One goal of the paper is similar to [17]: is it possible to understand multiply connected Hall plates with the classical theory of Maxwell? We will use a more general and more rigid mathematical approach than Oszwaldowski *et al.*, but the conclusion is the same: yes. However, it may be cumbersome to obtain numerical values with methods of analytical calculation. Even at zero magnetic field the general relation between resistivity and voltages measured between peripheral contacts in a plane plate with a hole is difficult. Attempts and a conjecture are given in [18] [19].

In fact the authors in [17] did not give an *ab initio* explanation for the Hall effect in doubly connected regions. They interpreted the regions near the four contacts as four separate Hall crosses. The two Hall crosses at the current supply contacts are operated in an unusual way: current enters in one branch of the cross, then it is split up and exits through the neighboring branches, while the fourth branch is not connected. In [17] the authors found experimentally that these two Hall crosses add certain voltages to the left and right branches of the ring, which are identical to half of the Hall voltages on the left and right Hall crosses, respectively. Adding up all voltages gives the correct Hall voltage as observed in [17] and also in [10]. However, the main question is still open: why do the two Hall crosses at the supply contacts add exactly the required voltages to match the experiments in [10]? Also the exact way how to add up the voltage contributions is obscure. These questions are not tackled in [17]—the following paper answers them in a rigorous mathematical framework.

In this paper we do not discuss quantum Hall effect phenomena, which are frequently mentioned in the context of multiply connected Hall effect regions [20]. We stay within the realm of classical stationary flow of electric current on a macroscopic scale in 2D.

Section 2 explains the “anti-Hall bar within a Hall bar” whose unexpected behavior bewildered several engineers with decades of experience in Hall sensor technology (including the author). **Section 3** states the assumptions of the theory. **Section 4** presents numerical simulations on a very general doubly connected device to give us an idea of the roles of symmetry, contacts size, and magnetic field strength. **Section 5** develops a theory for Hall plates, where all boundaries are insulating. **Sections 6–8** apply this theory to simply-connected, doubly-connected, and multiply-connected plane Hall plates without interior current sources. **Section 9** explains the role of extended contacts in the limit of large applied magnetic field. **Section 10** sums up the main achievements of the paper. In **Appendix A** we compute the current pattern in the unit disk with and without hole, if point current contacts are on the unit circle.

2. The “Anti-Hall Bar within a Hall Bar”: A Surprising Example Kindles Our Interest

In [10] a rectangular Hall plate with a symmetric rectangular hole was discussed. We repeat the calculation with the commercial finite element (FEM) code COMSOL

MULTIPHYSICS. The geometry of such an “anti-Hall bar within a Hall bar” is shown in **Figure 1(a)**. There the conductive region is a symmetric ring with the outer boundary being a 14×2 rectangle and the inner rectangular hole boundary is 13.6×1 large (the units are arbitrary). We intentionally exaggerate the aspect ratio of the device to emphasize the astonishing result. The model is 2D with the thickness normalized to 1. Let us also normalize the resistivity to $\rho = 1 \Omega \cdot \text{m}$. The resistivity tensor ρ describing the Hall effect in this static conduction problem is simply

$$\begin{pmatrix} E_x \\ E_y \end{pmatrix} = \rho \begin{pmatrix} J_x \\ J_y \end{pmatrix} \quad \text{with} \quad \rho = \rho \begin{pmatrix} 1 & \mu_H B_{a,z} \\ -\mu_H B_{a,z} & 1 \end{pmatrix} \quad (1)$$

All boundaries are insulating and a current of 1 Ampere is injected into the device at the left outer boundary in point A. The current is extracted at the opposite point B also being on the outer boundary. We are interested in the potential at points C, D, E, F on the vertical symmetry line with C and F on the outer boundary and D and E on the inner boundary. We are free to choose one point as reference point for the potential and so we ground D. For good accuracy a fine mesh with 1.9 million elements was used. The applied magnetic field was swept from $\mu_H B_{a,z} = -1.28$ to 1.28. For the largest magnetic field the current

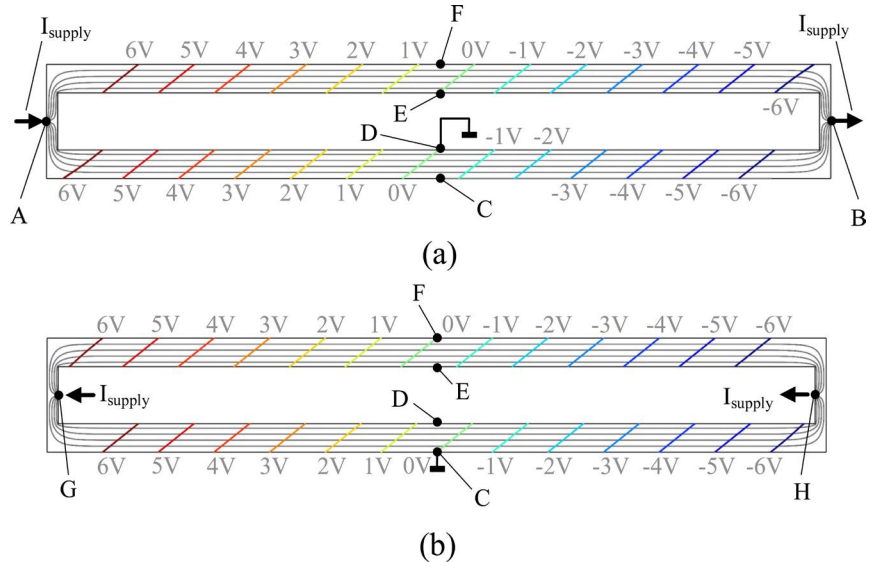


Figure 1. An “anti-Hall bar within a Hall bar” is a rectangular Hall plate with a rectangular, symmetric hole and point sized contacts. In (a) the current is supplied at points A, B on the outer perimeter, whereas in (b) the current is supplied at points G, H on the inner perimeter. The output contacts are at points C, D, E, F. In (a) point D is grounded, whereas in (b) point C is grounded. The supply current is 1 A and the applied magnetic field is strong (52° Hall angle). The figures show current streamlines (grey color) and the identical color coding denotes the values of the electric potential (red means $+6$ V, green is 0 V, blue is -6 V, also labelled). The slanting of the contour lines is identical in (a) and (b). Yet in (a) and (b) the contours in the upper branch are shifted differently in horizontal direction against the contours in the lower branch, such that potentials in D and E are identical in (a) yet potentials in C and F are identical in (b). Thus, in (a) there is no Hall voltage between D-E, whereas in (b) there is no Hall voltage between C-F.

streamlines are shown in grey color and the contours of the potential are drawn in color. The current streamlines are parallel in the upper and lower horizontal parts of the device, and there the contours of the potential are also straight lines tilted against the current streamlines by 90° minus the Hall angle. This is identical to simply connected Hall plates. In **Figure 2(a)** we plot the potential at the four points C, D, E, F. At zero magnetic field the potential is identical at all four points due to symmetry. With rising magnetic field the potential at the lower point C on the outer boundary decreases while the potential at the upper point F on the outer boundary increases. This gives an increasing output voltage between C and F in exactly the same way as it occurs in simply connected Hall plates. However, the potentials in the points D and E at the inner boundary remain zero versus magnetic field. Thus, *the voltage between D and E does not respond to an applied magnetic field of arbitrary strength*.

In **Figure 1(b)** we inject the current at point G and extract it at point H. Both points are on the inner boundary. Then the potentials in D and E on the inner boundary respond to applied magnetic field, whereas the voltage between points C and F on the outer boundary does not respond to applied magnetic field (see **Figure 2(b)**). Hence, the stunning result is that the voltage between C and F depends on whether the current is supplied via points on the inner or outer boundary, although the current streamlines near C and F are perfectly horizontal in both cases. This holds even if the aspect ratio of the device becomes infinite and the points of current injection move to left and right infinity—nevertheless at applied magnetic field the voltage between C and F changes markedly if we swap the current contacts between inner and outer boundaries. These numerical findings are in perfect agreement to experimental observations [21]. In this paper we try to clarify this phenomenon. In particular we ask if this behavior is valid only for certain symmetries, for single holes (single ring topologies), or for

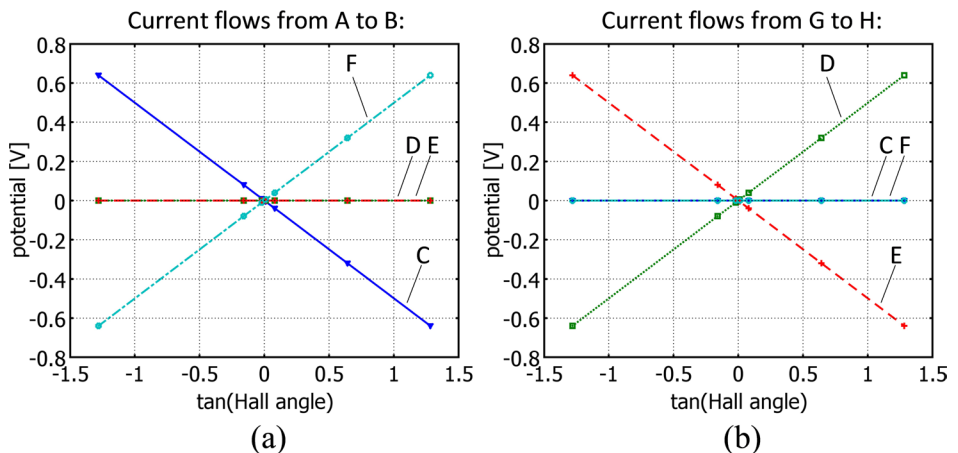


Figure 2. The electric potential at points C, D, E, F of the Hall plate with hole in **Figure 1** versus tangent of Hall angle ($= \mu_H B_{a,z}$): (a) shows the potential for current flowing through the outer contacts A-B in **Figure 1(a)**, whereas (b) shows the potential for current flowing through the inner contacts G-H in **Figure 1(b)**. The stunning result is that the Hall voltage vanishes on inner contacts D-E if current is supplied via outer contacts A-B, and vice versa.

point-sized contacts.

3. Assumptions and Basic Definitions

In this paper we deal only with plane Hall plates whose size in the (x, y) -plane is much larger than their small and homogeneous thickness t_H in z -direction. All quantities are constant versus z -position: $\partial/\partial z = 0$. A magnetic flux density \mathbf{B}_a is applied with external means to the Hall plate. It has a component only in z -direction $\mathbf{B}_a = B_{a,z} \mathbf{n}_z$ (\mathbf{n}_z is the unit vector in z -direction) and it is homogeneous in the entire (x, y) -plane. It may be weak but it may also be very large. Then the classical Hall effect is described by

$$\mathbf{E} = \rho \mathbf{J} + \rho \mu_H \mathbf{J} \times \mathbf{B}_a \quad (2a)$$

$$\mathbf{J} = \frac{\mathbf{E} - \mu_H \mathbf{E} \times \mathbf{B}_a + \mu_H^2 (\mathbf{E} \cdot \mathbf{B}_a) \mathbf{B}_a}{\rho (1 + \mu_H^2 |\mathbf{B}_a|^2)} \rightarrow \frac{\mathbf{E} - \mu_H \mathbf{E} \times \mathbf{B}_a}{\rho (1 + \mu_H^2 B_{a,z}^2)} \quad (2b)$$

with the specific ohmic resistivity $\rho > 0$ and the Hall mobility $\mu_H > 0$. These two material parameters are assumed to be constant versus space and versus electric and magnetic fields. They are both assumed to be simple scalars. The positive mobility in (2a, b) is valid for electrons as majority carriers—for holes we have to use a negative mobility. We assume only a single dominant type of charge carrier. Equation (2b) follows from (2a) if \mathbf{B}_a is perpendicular to the thin Hall plate. Its derivation is given in [22]. The electric field \mathbf{E} and the current density \mathbf{J} have no z -component. $\mathbf{J} \times \mathbf{B}_a$ denotes the vector product of \mathbf{J} and \mathbf{B}_a . $\mathbf{E} \cdot \mathbf{B}_a$ is the scalar product of \mathbf{E} and \mathbf{B}_a .

We consider Hall plates with four contacts, the contacts having infinite conductivity. Via two supply contacts we force a current I_{supply} through the Hall plate and at the other two sense contacts we tap an output voltage V_{out} . Perfectly symmetric Hall plates have zero output voltage at zero magnetic field. However, in practice Hall plates always suffer from unavoidable asymmetries so that in general one has to account for a non-vanishing output voltage in the absence of applied magnetic field—this is called offset. If magnetic field is applied the output voltage will change. We decompose the output voltage into a sum of even and odd functions of the applied magnetic field. The even part is commonly called the offset and the odd part is the Hall voltage V_H .

$$V_{\text{out}}(B_{a,z}) = V_{\text{even}}(B_{a,z}) + V_{\text{odd}}(B_{a,z}) \quad (3a)$$

$$V_{\text{even}}(B_{a,z}) = \frac{V_{\text{out}}(B_{a,z}) + V_{\text{out}}(-B_{a,z})}{2} \quad (3b)$$

$$V_{\text{odd}}(B_{a,z}) = V_H(B_{a,z}) = \frac{V_{\text{out}}(B_{a,z}) - V_{\text{out}}(-B_{a,z})}{2} \quad (3c)$$

$V_{\text{out}}(B_{a,z})$ is measured at positive applied magnetic field and $V_{\text{out}}(-B_{a,z})$ is measured at negative applied magnetic field. With the principle of reverse magnetic field reciprocity (RMFR [23] [24] [25]) one can show that $V_{\text{out}}(-B_{a,z})$ is identical to the output voltage tapped between the supply contacts when current

is sent through the sense contacts at positive applied magnetic field. In a strict sense this holds only in an electrically linear and isothermal device (no junction isolation at the insulating boundaries, no velocity saturation, no self-heating, no self-magnetic field, and no thermo-magnetic effects). Then the Hall voltage V_H is equal to the output of a spinning current Hall scheme [26] [27] [28], and we do not need to reverse the polarity of the applied magnetic field to obtain it. This principle is used in most smart Hall sensor ASICs because it improves the zero-point error by a factor of ~500 [29].

We can also measure the potential ϕ with a single point-sized probe at any location \mathbf{r} in the Hall plate. Analogous to (3a-c) we define the even potential ϕ_{even} and the odd potential ϕ_{odd} (=Hall potential ϕ_H)

$$\phi(\mathbf{r}, B_{a,z}) = \phi_{\text{even}}(\mathbf{r}, B_{a,z}) + \phi_{\text{odd}}(\mathbf{r}, B_{a,z}) \quad (4a)$$

$$\phi_{\text{even}}(\mathbf{r}, B_{a,z}) = \frac{\phi(\mathbf{r}, B_{a,z}) + \phi(\mathbf{r}, -B_{a,z})}{2} \quad (4b)$$

$$\phi_{\text{odd}}(\mathbf{r}, B_{a,z}) = \phi_H(\mathbf{r}, B_{a,z}) = \frac{\phi(\mathbf{r}, B_{a,z}) - \phi(\mathbf{r}, -B_{a,z})}{2} \quad (4c)$$

If the location \mathbf{r}_1 is on the first sense contact and \mathbf{r}_2 on the second sense contact then $V_{H,12} = \phi_H(\mathbf{r}_1) - \phi_H(\mathbf{r}_2)$. Other authors define the Hall potential as the difference of potential with and without magnetic field, which differs from our definition by the magnetic field change of offset $(\phi(B_{a,z}) + \phi(-B_{a,z})) / 2 - \phi(B_{a,z} = 0)$. This difference is small of order $O^2(B_{a,z})$ for small magnetic field.

All odd functions vanish at zero applied magnetic field due to their definition.

$$V_{\text{odd}}(0) = 0, \phi_{\text{odd}}(\mathbf{r}, 0) = 0 \quad (5)$$

We denote all even functions at zero applied magnetic field with an index 0

$$V_{\text{out}}(0) = V_{\text{even}}(0) = V_{\text{out},0} \quad (6a)$$

$$\phi(\mathbf{r}, 0) = \phi_{\text{even}}(\mathbf{r}, 0) = \phi_0(\mathbf{r}) \quad (6b)$$

$$\mathbf{E}(\mathbf{r}, 0) = \mathbf{E}_0(\mathbf{r}) \quad (6c)$$

$$\mathbf{J}(\mathbf{r}, 0) = \mathbf{J}_0(\mathbf{r}) \quad (6d)$$

The Hall voltage depends on the supply current through the Hall plate, the magnetic field applied to the Hall plate, and on the material parameters and the geometry of the Hall plate. The literature on Hall plates casts this relation into the following form

$$V_H = I_{\text{supply}} R_{\text{sheet}} G_H \tan \theta_H \quad (7)$$

with the sheet resistance $R_{\text{sheet}} = \rho/t_H$, the Hall geometry factor G_H , and the Hall angle θ_H . In the entire Hall plate the electric field vectors \mathbf{E} are rotated by the angle θ_H against the current density vectors \mathbf{J} , as can be seen in (2). From (2) we get $\tan \theta_H = \mu_H B_{a,z}$. Small magnetic field means $\theta_H \approx 0^\circ$, and large magnetic field means $\theta_H \rightarrow \pm 90^\circ$ depending on the polarity of the magnetic field. The Hall geometry factor summarizes all effects caused by the geo-

metry of the Hall plate and the finite size of its contacts. It holds $0 \leq G_H \leq 1$. If all four contacts are point-sized and peripheral $G_H = 1$ (see also (19)). The larger the contacts, the smaller G_H . Therefore G_H describes the reduction of the magnetic sensitivity of a Hall plate caused by its contacts. The sense contacts shunt a part of the supply current away from the interior of the Hall plate so that not all the current is available for the Hall effect. And the supply contacts have a short circuiting effect on the Hall electric field which hinders the Hall voltage to develop unrestrained between the sense contacts. Due to an interplay between magnetic field and geometry at the contacts (see **Section 9**), in general G_H is also a function of θ_H . At large magnetic field $G_H \rightarrow 1$ regardless of the size of the contacts. That means at large magnetic field all contacts behave similar to point contacts. In this paper we will keep the definition (7) of the Hall geometry factor, but expand its range of validity to Hall plates with holes with $-1 \leq G_H \leq 1$. Note that the Hall voltage is sampled between two points $V_{H,12} = \phi_H(\mathbf{r}_1) - \phi_H(\mathbf{r}_2)$, and therefore the Hall geometry factor also relates to these two points $G_H = G_{H,12}$. However, we can ground one of these points and then the Hall geometry factor can be interpreted as a normalized Hall potential $G_H(\mathbf{r}_1) = \phi_H(\mathbf{r}_1) / (I_{\text{supply}} R_{\text{sheet}} \tan \theta_H)$ for $\phi(\mathbf{r}_2) = 0 \Rightarrow \phi_H(\mathbf{r}_2) = 0$.

4. Doubly-Connected Asymmetric Hall Plates with Large Contacts

In **Figure 3(a)** we have an entirely asymmetric Hall plate with asymmetric hole. It has two large contacts for current supply at the outer boundary and two large sense contacts on the inner boundary. **Figure 3(b)** shows the same Hall plate, but now the contacts on the inner boundary became insulating edges, and instead we added two large sense contacts on the outer boundary. Both figures show potential and current streamlines at large magnetic field ($\mu_H B_{a,z} = 1.28$): obviously the current streamlines are not perpendicular to the contacts. In both cases (a) and (b) we ground the right sense contact and observe how the potential at the left sense contact responds to applied magnetic field. This is shown in **Figure 3(c)**. Evidently there is a response regardless if the contacts are on the inner or outer boundary. The slope $|dV_{\text{out}}/dB_{a,z}|$ decreases at large magnetic field for contacts on the inner boundary (sub-linear growth), whereas it increases versus magnetic field for contacts on the outer boundary (super-linear growth). This becomes more apparent if we compute the Hall geometry factor G_H according to its definition in (7), again with the rule that the sense contact at the RHS of global current flow between current contacts is grounded. **Figure 3(d)** shows G_H for both cases of inner and outer sense contacts: in the limit of very strong magnetic field $G_H \rightarrow 1$ for outer sense contacts whereas $G_H \rightarrow 0$ for inner sense contacts. Note that G_H is fairly constant for $|\tan \theta_H| < 1$. This is the condition under which one usually likes to operate Hall devices as magnetic field sensors, because of their linear response to applied magnetic field. However, for high mobility materials like graphen or InSb it may happen that

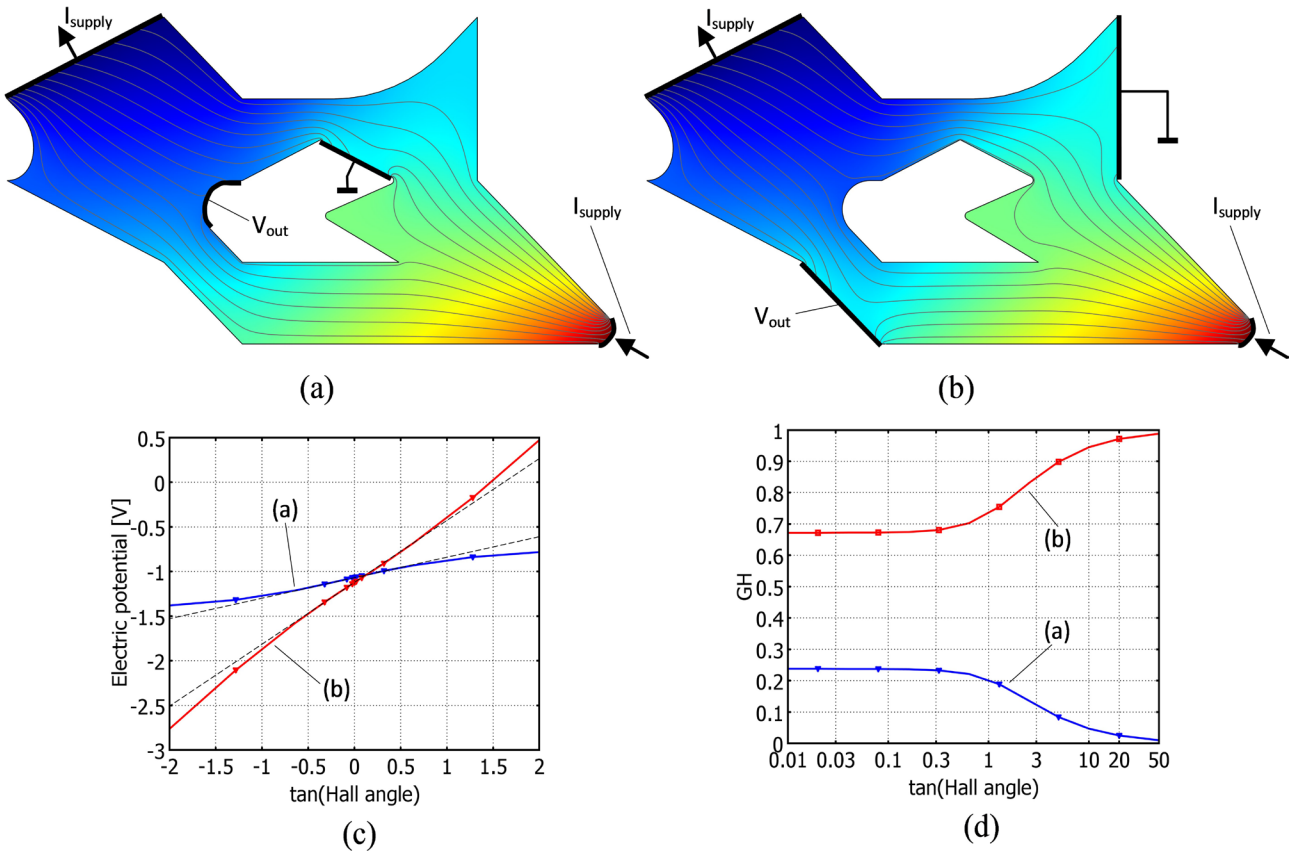


Figure 3. Asymmetric Hall plate with hole and with four large contacts (=thick black lines). Current contacts are on the outer boundary. Sense contacts are on the inner boundary in (a) and on the outer boundary in (b). The right sense contact is grounded. The figures (a, b) show current streamlines (grey color) at large magnetic field (52° Hall angle). The color coding denotes the values of the electric potential (red means positive, blue is negative potential). (c): electric potential of the non-grounded sense contacts of Figures (a) and (b) versus tangent of Hall angle ($= \mu_H B_{a,z}$). The straight dashed lines are to guide the eye. (d) Hall geometry factor of the non-grounded sense contacts of Figures (a) and (b) versus tangent of Hall angle.

$|\tan \theta_H| > 1$. Then one may use a doubly connected Hall plate like in **Figure 3** where the ratio of Hall voltages in (a) and (b) is a unique function of $\mu_H B_{a,z}$. This could be used in an auto-calibration scheme of a smart sensor system. To sum up, *the behavior on inner and outer sense contacts for this asymmetric Hall plate with large contacts differs, but the difference is milder than in Figure 1*: the Hall response is smaller on the inner contacts but it does not vanish altogether unless the magnetic field grows unboundedly.

If we make one current contact point sized, skip the large sense contacts, and sample the Hall potential only with point probes, the behavior is similar. **Figure 4(a)** shows the potential and the current streamlines at large magnetic field and **Figure 4(b)** shows the geometry factor for output voltages at various points on the inner boundary. Point 17 is grounded. All other points labeled in **Figure 4(a)** along the hole boundary have non-vanishing Hall voltage. Most points show negative Hall geometry factor, except for points 7, 10, and 12. But *the Hall geometry factor at all points in the hole boundary tends to zero at large Hall angle*. **Figure 4(c)** shows the Hall geometry factor for several points on the outer

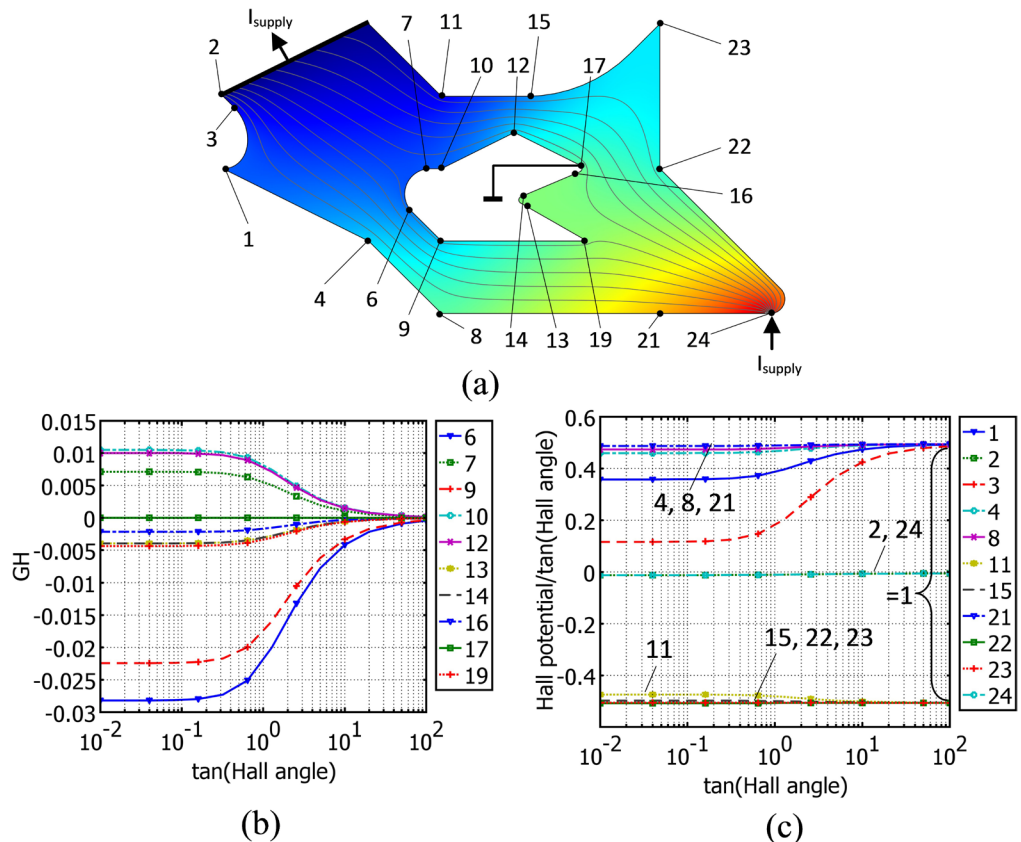


Figure 4. (a) Hall plate similar to **Figure 3**, yet with point sized current injection and point sized sense contacts. Only the current sink contact is large. Current streamlines and potential are shown for large positive magnetic field (52° Hall angle). Several points on the boundary are indicated. One of them (point 17) is grounded; (b) Hall geometry factor G_H on several points on the hole boundary versus tangent of Hall angle ($= \mu_H B_{a,z}$); (c) Hall potential divided by tangent of Hall angle is plotted versus tangent of Hall angle for all indicated points on the outer boundary (for $I_{\text{supply}} = 1\text{A}$, $R_{\text{sheet}} = 1\Omega$).

boundary. As we grounded an inner point, the Hall geometry factor for the outer points is not between 0 and 1 but between approximately -0.5 and 0.5 (only for this specific example)—therefore we plotted the Hall potential over tangent of Hall angle at 1 Ampere supply current and 1 Ohm sheet resistance. Anyhow, if one taps the output voltage between a point on the left outer boundary and a point on the right outer boundary its G_H goes to 1 for large magnetic fields.

Finally, if we replace the last big contact in **Figure 4(a)** with a point contact, the situation changes drastically as shown in **Figure 5**: 1) the Hall potential on all points along the inner boundary is identical, 2) the Hall potential on all points along the left perimeter between the current contacts is identical, and 3) the Hall potential on all points along the right perimeter between the current contacts is identical. The Hall geometry factor between any two points on the inner boundary vanishes, whereas the Hall geometry factor between any point left of the current injection and any point right of the current injection equals 1. Therefore, *the particular behavior of the “anti-Hall bar within a Hall bar” seems to have two origins: in the case of irregular geometry it is the infinitely small*

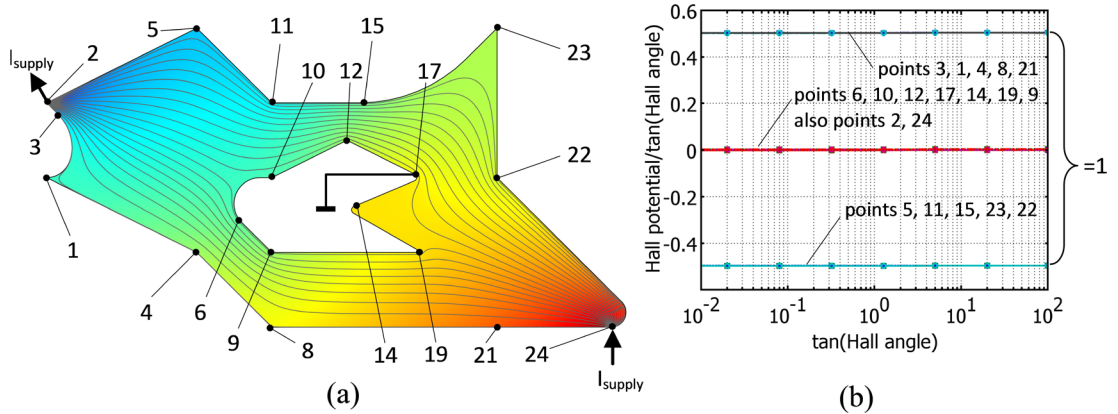


Figure 5. (a) The same Hall plate as in [Figure 3](#), yet with all contacts being point sized. Current streamlines and potential are shown for large positive magnetic field (52° Hall angle). Several points on the boundary are indicated. One of them (point 17) is grounded; (b) Hall potential divided by tangent of Hall angle is plotted versus tangent of Hall angle for all indicated points (for $I_{\text{supply}} = 1\text{A}$, $R_{\text{sheet}} = 1\Omega$): it is zero for all points on the hole boundary, positive for points left of the global current flow, and negative for points right of it. The difference of values between left and right points is equal to 1.

contacts, and in the case of large contacts it is the symmetry according to Haeusler [9].

5. Plane Hall Plates Where All Boundaries Are Insulating

If all boundaries are insulating the contacts must be point sized. Then it is better to use the stream function instead of the potential, because the boundary conditions specify the stream function and not the potential (see also [Appendix A](#)).

However, the stream function exists only in a limited class of topologies where the net current through every closed curve inside a multiply connected domain vanishes (regardless if the contacts are point sized or extended).

$$\oint_C \mathbf{J} \cdot \mathbf{n} ds = 0 \Leftrightarrow \text{stream function exists} \quad (8)$$

with \mathbf{n} being the unit vector perpendicular to the curve. Thereby the closed curve may also encircle holes. If a multiply-connected Hall plate has one current input contact and one current output contact and both are on the boundary of the same hole, a stream function exists. The same holds if both contacts are on the outer perimeter. If the current input contact is on the boundary of a different hole than the current output contact, no stream function exists. If the entire boundary of a hole is a single current contact, no stream function exists. This holds also in the limit of vanishing hole size. Topologies with no stream function will be focused on in the follow-up part II of this publication. A proof of (8) will become clear later (see (18)).

According to Maxwell's first equation in the quasi-static case it holds

$$\mathbf{J} = \nabla \times \mathbf{H} = \begin{pmatrix} \partial H_z / \partial y - \partial H_y / \partial z \\ \partial H_x / \partial z - \partial H_z / \partial x \\ \partial H_y / \partial x - \partial H_x / \partial y \end{pmatrix} \quad (9)$$

with the magnetic field \mathbf{H} linked to the current flow. Note that \mathbf{H} is the magnetic field that is generated by the current streamlines—it is not the magnetic field applied to the Hall plate $\mu_0 \mathbf{H} \neq \mathbf{B}_a$. Most of the literature on the Hall effect tacitly assumes $\mu_0 |\mathbf{H}| \ll |\mathbf{B}_a|$, i.e., the magnetic field caused by the current through the Hall plate is thought to be negligible against the externally applied magnetic field. With (9) the divergence of the current density vanishes

$$\nabla \cdot \mathbf{J} = 0 \quad (10)$$

because $\nabla \cdot \nabla \times \mathbf{H} = \nabla \times \nabla \cdot \mathbf{H} = 0$. In a thin plane Hall plate it holds: 1) $J_z = 0$, 2) $\partial J_x / \partial z = \partial J_y / \partial z = 0$, and 3) J_x, J_y generate no H_x, H_y within the conductive region. Therefore H_z is the only non-zero component in the conductive region. It defines the stream function

$$\psi = -\rho H_z \quad (11)$$

In (11) the resistivity makes the dimensions of stream function and potential equal in order to combine them to the complex potential, and the minus sign makes this complex potential compliant with the Cauchy-Riemann differential equations in the case $B_{a,z} = 0$ (see (20a, b) below).

In (9)-(11) we adopted a three-dimensional picture how \mathbf{J} and \mathbf{H} are linked. Due to the small thickness of the Hall plate several components of the vector fields vanish. The non-vanishing quantities are sufficient to define a consistent two-dimensional model where H_z is a function of J_x, J_y . Such a 2D problem in the (x, y) -plane implicitly assumes $\partial / \partial z = 0$ for all quantities, and this implies an infinitely thick Hall plate $t_H \rightarrow \infty$ with $J_z = 0$. Therefore it assumes $H_x = H_y = 0$ —not only inside the Hall plate but everywhere. Then the point current contacts become line contacts parallel to the z -axis. It is important to keep in mind that in such a 2D problem $-\psi / \rho$ is the magnetic field H_z of the currents in an infinitely thick Hall plate, and not in the real, thin Hall plate (for the same current pattern J_x, J_y with $J_z = 0$ the magnetic field in thick and thin Hall plates differs in $z = 0$, which becomes apparent if we insert the current density into the law of Biot-Savart to compute the magnetic field:

$$\mathbf{H}(\mathbf{r}) = \frac{1}{4\pi} \int_{A'} \int_{z'} \mathbf{J}(\mathbf{r}') \times \frac{\mathbf{r} - \mathbf{r}'}{|\mathbf{r} - \mathbf{r}'|^3} dA' dz' \quad (12)$$

A' is the area in the (x, y) -plane. For the thick Hall plate the integration goes $z' : -\infty \rightarrow \infty$ whereas for the thin Hall plate it goes only $z' : \lim_{t_H \rightarrow 0} -t_H/2 \rightarrow t_H/2$ which is a simple multiplication by t_H .

Since \mathbf{J} is obtained from H_z by spatial differentiation in (9), and H_z is proportional to ψ in (11), the stream function ψ takes over the role of a 2D “potential” that can be used in a way similar to the potential ϕ . It holds

$$\mathbf{J} = -\nabla \times \frac{\psi \mathbf{n}_z}{\rho} = \frac{-1}{\rho} \frac{\partial \psi}{\partial y} \mathbf{n}_x + \frac{1}{\rho} \frac{\partial \psi}{\partial x} \mathbf{n}_y \quad (13)$$

$\mathbf{n}_x, \mathbf{n}_y, \mathbf{n}_z$ are the Cartesian unit vectors. Note the different viewpoint: in (9) \mathbf{H} is generated by \mathbf{J} , yet in (13) \mathbf{J} is generated by ψ . In fact both equations

just describe how the quantities $\mathbf{H}, \mathbf{J}, \psi$ are linked without causality: they do not differentiate between origin and reaction.

Defining \mathbf{J} as the curl of $-(\psi/\rho)\mathbf{n}_z$ implies that \mathbf{J} is orthogonal to $\nabla\psi$

$$\mathbf{J} \cdot \nabla\psi = \frac{1}{\rho} \left(\begin{array}{c} -\partial\psi/\partial y \\ \partial\psi/\partial x \\ \partial\psi/\partial y \end{array} \right) \cdot \left(\begin{array}{c} \partial\psi/\partial x \\ \partial\psi/\partial y \\ \partial\psi/\partial z \end{array} \right) = 0 \quad (14)$$

This explains the name stream function, because it is *constant along each current streamline*. With Maxwell's second equation and (2a) we get

$$\nabla \times \mathbf{E} = \mathbf{0} = \rho \nabla \times \mathbf{J} + \rho \mu_H B_{a,z} \nabla \times (\mathbf{J} \times \mathbf{n}_z) \quad (15)$$

$\nabla \times (\mathbf{J} \times \mathbf{n}_z) = (\mathbf{n}_z \cdot \nabla) \mathbf{J} - \mathbf{n}_z (\nabla \cdot \mathbf{J}) = \mathbf{0}$ because of $\mathbf{n}_z \cdot \nabla = 0$ for 2D geometries and because of (10). With

$\rho \nabla \times \mathbf{J} = -\nabla \times (\nabla \times \psi \mathbf{n}_z) = -\nabla(\nabla \cdot \mathbf{n}_z \psi) + \nabla^2 \psi \mathbf{n}_z = \nabla^2 \psi \mathbf{n}_z$ we conclude that the stream function must also fulfill Laplace's equation $\nabla^2 \psi = 0$. The boundary conditions at extended contacts are $\partial\psi/\partial n = \mu_H B_{a,z} \partial\psi/\partial t$ and at the insulating boundary the normal current density vanishes. Thus it holds $\partial\psi/\partial t = 0$ and therefore ψ is *constant on insulating boundaries*. This goes along with the notion that along any insulating boundary there flows one specific current streamline and the stream function is constant on current streamlines, thus, it is also constant along the insulating boundary.

Both ϕ and ψ are solutions of the Laplace equation, yet the Laplace equation is independent of the applied magnetic field. The magnetic field dependence of potential and current distribution is determined by the boundary conditions only. Hence, one might speculate that the volume is less important than the boundary for the Hall effect. After all, there is no Hall voltage in an infinitely large, unbounded Hall plate (cf. Figure 5(a) and Figure 6(c) in [30]). On the other hand the Lorentz force acts on the charge carriers in the whole volume. Thus the Hall effect appears to be a peculiar interplay between volume and boundary.

If a Hall plate has only insulating boundaries and point-sized contacts where current is impressed, both the Laplace equation and the boundary conditions for the stream function do not contain the applied magnetic field any more. *In such a Hall plate the stream function, the current density, and the current streamlines are constant versus applied magnetic field*. For the case of a circular disk with peripheral point current contacts this was already stated in [30]. Now we see that it is also valid for multiply-connected regions with point sized contacts whenever a stream function exists.

If we express the electric field in (2a) by the potential and the current density by the stream function this gives

$$\nabla\phi = \nabla \times \psi \mathbf{n}_z - \mu_H B_{a,z} \nabla\psi \quad (16a)$$

At vanishing applied magnetic field (16a) reads

$$\nabla\phi_0 = \nabla \times \psi \mathbf{n}_z \quad (16b)$$

For the particular case of all-insulating boundaries we do not need an index 0

for ψ , because it is identical with and without applied magnetic field. From (16a, b) we get

$$\nabla \phi = \nabla \phi_0 - \mu_H B_{a,z} \nabla \psi \Rightarrow \phi = \phi_0 - \mu_H B_{a,z} (\psi - \psi_{\text{ground}}) \quad (16c)$$

In the ground node it holds $\phi = \phi_0 = 0$ and therefore $\psi = \psi_{\text{ground}}$. We are free to choose ψ_{ground} and so we define $\psi_{\text{ground}} = 0$, which means $\psi = 0$ in the ground node. With this convention, with (4a), (16c), and with the fact that ψ is independent of $B_{a,z}$ the Hall potential becomes

$$\phi_H = -\mu_H B_{a,z} \psi \quad (17a)$$

Thus, *the Hall potential is constant along current streamlines*, and the Hall voltage between two points is simply proportional to the difference in stream function

$$V_{H,12} = \phi_{H1} - \phi_{H2} = -\mu_H B_{a,z} (\psi_1 - \psi_2) \quad (17b)$$

Another property of the stream function is its relation to the total current I_{12} flowing across any contour (extruded into thickness direction) that starts at point 1 and ends at point 2. Using (13) we get

$$\begin{aligned} I_{12} &= t_H \int_1^2 J_n ds = t_H \mathbf{n}_z \cdot \int_1^2 \mathbf{J} \times \mathbf{t} ds = -\frac{t_H}{\rho} \int_1^2 \frac{\partial \psi}{\partial x} dx + \frac{\partial \psi}{\partial y} dy \\ &= -\frac{t_H}{\rho} \int_1^2 d\psi = -\frac{\psi_2 - \psi_1}{R_{\text{sheet}}} \end{aligned} \quad (18)$$

whereby we used $J_n = \mathbf{J} \cdot \mathbf{n}$, $\mathbf{n} = \mathbf{t} \times \mathbf{n}_z$, $\mathbf{n} \cdot \mathbf{n} = \mathbf{t} \cdot \mathbf{t} = 1$, and \mathbf{t} is tangential to the path and points from point 1 to point 2. The current I_{12} flowing across the contour connecting the two points 1, 2 is the difference in stream function at these two points divided by the sheet resistance. Inserting (18) into (17b) and comparing with (7) gives

$$G_{H,12} = \frac{\phi_{H1} - \phi_{H2}}{I_{\text{supply}} R_{\text{sheet}} \mu_H B_{a,z}} = \frac{-I_{12}}{I_{\text{supply}}} \quad (19)$$

Thus, *the Hall geometry factor between the points 1 and 2 is equal to the ratio of the current between the two points and the total current through the Hall plate*. This holds for multiply connected conductive regions without extended contacts and without internal current sources (*i.e.*, whenever a stream function exists). Obviously, 1) this ratio cannot exceed 1 and it is smaller if both points 1, 2 are in the interior of the Hall plate with peripheral contacts, 2) it is zero along any insulating boundary without current contacts between points 1 and 2, and 3) it is ± 1 if points 1 and 2 are on the same boundary and a single point-sized supply contact is between them on this boundary.

In Hall plates with all insulating boundaries and point sized contacts the current pattern does not change with applied magnetic field (see above). Therefore (19) implies that the Hall geometry factor is constant versus applied magnetic field. Consequently the Hall voltage is directly proportional to the applied magnetic field whenever the current through the Hall plate is kept constant. *These*

devices are linear versus applied magnetic field—within the scope of our assumption that the material parameters ρ, μ_H are constant. In engineering practice one may partly compensate for the magnetic field dependence of the material parameters with the magnetic field dependence of the Hall geometry factor in Hall plates with extended contacts [31].

If the integration path in (18) is a closed loop, points 1 and 2 are identical and this leads to (8). Hence, we see that in multiply-connected domains a stream function makes sense only in the absence of internal current sinks and sources.

The stream function jumps in point-sized current contacts according to (18), and so we must not use it there, because it would lead to self-contradictory predictions. Let us assume point 1 exactly at the current contact and point 2 somewhere inside the Hall plate. If we would erroneously apply (18), this gives $\psi_2 = \psi_1$ because obviously $I_{12} = 0$ (both points are on a current streamline and therefore no current flows across this streamline). This would mean that the stream function is constant everywhere inside the Hall plate—which of course is wrong. If ψ is discontinuous in a point-sized current contact also ϕ_H is discontinuous there according to (17a). Hence, also ϕ_H makes no sense in point contacts. On the other hand we can sample the Hall voltage between two points on the same current streamline and it vanishes according to (17b). If the two points approach positive and negative supply contacts it still holds $V_H = 0$. Hence, the Hall voltage across supply contacts vanishes. The argument holds for point-sized supply contacts, but the Hall voltage also vanishes across extended supply contacts (this can be shown with the methods developed in [32]).

In the absence of an applied magnetic field ($B_{z,a} = 0$) it holds

$$E_x = \rho J_x \Rightarrow \frac{\partial \phi_0}{\partial x} = \frac{\partial \psi}{\partial y} \quad (20a)$$

$$E_y = \rho J_y \Rightarrow \frac{\partial \phi_0}{\partial y} = -\frac{\partial \psi}{\partial x} \quad (20b)$$

These are the Cauchy-Riemann differential equations and therefore the functions $F_{R0} = \phi_0 + i\psi$ and $F_{I0} = -\psi + i\phi_0$ are analytic functions, which are commonly called complex potentials. (20a, b) imply $\nabla \phi_0 \cdot \nabla \psi = 0$, curves of constant ϕ_0 and curves of constant ψ are orthogonal. If we combine this with (17a) we arrive at the simple and well known fact that the gradient of the Hall potential is orthogonal to J_0 .

In the presence of an applied magnetic field E and J are not parallel, and therefore ϕ and ψ do not fulfill the Cauchy-Riemann differential equations. Nonetheless we can construct a complex potential whenever the stream function ψ exists. There are two possibilities: either the real or the imaginary part of the complex potential is equal to the electric potential ϕ , and the remainder is defined such as to satisfy the Cauchy-Riemann differential equations (enter (13), (16c), and $J = J_0$ into (2a)).

$$F_R = -iF_I = \phi + i(\mu_H B_{a,z}\phi + (1 + \mu_H^2 B_{a,z}^2)\psi) \quad (21)$$

Thus, the complex number F_I is equal to F_R rotated by 90° . (21) is valid for Hall plates with small and large contacts at applied magnetic field without internal current sources. For point sized contacts without internal current sources we can write (21) for positive and negative applied magnetic field with identical ψ . Subtracting both we get with (4b) and (17a)

$$F_{R,\text{odd}} = \frac{F_R(B_{a,z}) - F_R(-B_{a,z})}{2} = \phi_H + i\mu_H B_{a,z} \phi_{\text{even}} = \mu_H B_{a,z} (-\psi + i\phi_{\text{even}}) \quad (22)$$

(22) is again an analytical function. Since ψ does not depend on $B_{a,z}$ in the entire Hall plate also ϕ_{even} is constant versus applied magnetic field because they have to fulfill the Cauchy-Riemann differential equations. Comparison of (4a) with (16c) and (17a) gives $\phi_{\text{even}} = \phi_0$. The contour lines of ψ and $\phi_{\text{even}} = \phi_0$ are orthogonal. Contour lines of constant Hall potential are orthogonal to equipotential lines at zero applied magnetic field. Moreover, we have $\phi_H = \phi - \phi_{\text{even}} = \phi - \phi_0$, i.e., in this particular case the Hall potential is the change in potential with and without applied magnetic field. Finally we can write the complex potential in Hall plates with point contacts like this

$$F_R = -iF_I = \phi_0 - \mu_H B_{a,z} \psi + i(\mu_H B_{a,z} \phi_0 + \psi). \quad (23)$$

Hence, the complex potential has no quadratic dependence on applied magnetic field. This gives a simple relation between complex potentials with and without applied magnetic field.

$$F_R = F_{R0} (1 + i\mu_H B_{a,z}) = (F_{R0}/\cos \theta_H) \exp(i\theta_H). \quad (24)$$

(24) is compatible with (C9) in [15]. If we define a complex electric field by $E = E_x - iE_y$ it holds

$$E(z) = -\frac{d}{dz} F_R(z) = i \frac{d}{dz} F_I(z) = \frac{E_0(z)}{\cos \theta_H} \exp(i\theta_H) \quad (25)$$

with $z = x + iy$. If we define a complex current density by $J = J_x - iJ_y$ it holds

$$J(z) = \frac{1}{\rho} \cos \theta_H \exp(-i\theta_H) E(z) = \frac{1}{\rho} E_0(z) = J_0(z) \quad (26)$$

E_0 and J_0 are the complex electric field and the complex current density, respectively, at zero applied magnetic field. The leftmost equality in (26) is identical to (2a). If we take the conjugate of (26) we see that the current density is equal to the electric field rotated CCW by the Hall angle (and scaled in length and dimension).

In the review process of this paper the author became aware of [33]. In section 5 of [33] some of the above given arguments are used to explain the “anti-Hall bar” of [10] for irregular shapes and point-sized contacts. In [33] the authors based their arguments on the assumption that for point contacts the current density does not change with applied magnetic field—which holds only for cases, where a stream function exists (they did not explicitly refer to the concept of a stream function).

6. Hall Plates without Holes and with Point Current Contacts on the Boundary

Riemann's mapping theorem says that all simply connected bounded plane domains can be mapped onto the unit disk with a conformal transformation. Such a mapping is described by an analytical function and it preserves angles. The potentials at corresponding points are identical and also the currents into corresponding contacts are identical. The Hall angle between \mathbf{E} and \mathbf{J} is also identical, but \mathbf{E} and \mathbf{J} themselves are generally not identical. If we are only interested in the potential, we can limit the discussion to the circular unit disk of **Figure 6** where the current contacts are placed symmetrical to the x -axis and the rightmost point $(x, y) = (1, 0)$ is grounded—in accordance with our previous rule this point is at the RHS if we move along a current streamline. The current contacts split the boundary in two parts, left and right of the current flow. The Hall potential must be constant on each of these two segments, because no current passes through the segments. Since we grounded a point on the right segment, the Hall potential and thus the Hall geometry factor vanish there. On the left segment the Hall geometry factor is $G_H = 1$ according to (19), because for $I_{\text{supply}} > 0$ it holds $J_y > 0$ on the x -axis and this gives

$$I_{12} = t_H \mathbf{n}_z \cdot \int_1^2 \mathbf{J} \times d\mathbf{s} = t_H \mathbf{n}_z \cdot \mathbf{n}_y \times \mathbf{n}_x \int_{x=-1}^{x=1} J_y dx = -t_H \int_{x=-1}^{x=1} J_y dx = -I_{\text{supply}} \quad (27)$$

The Hall geometry factor between any two points *inside* the disk is smaller than 1. It can be computed in closed form (see **Appendix A**, compare also Figures 5 and 6 in [30]).

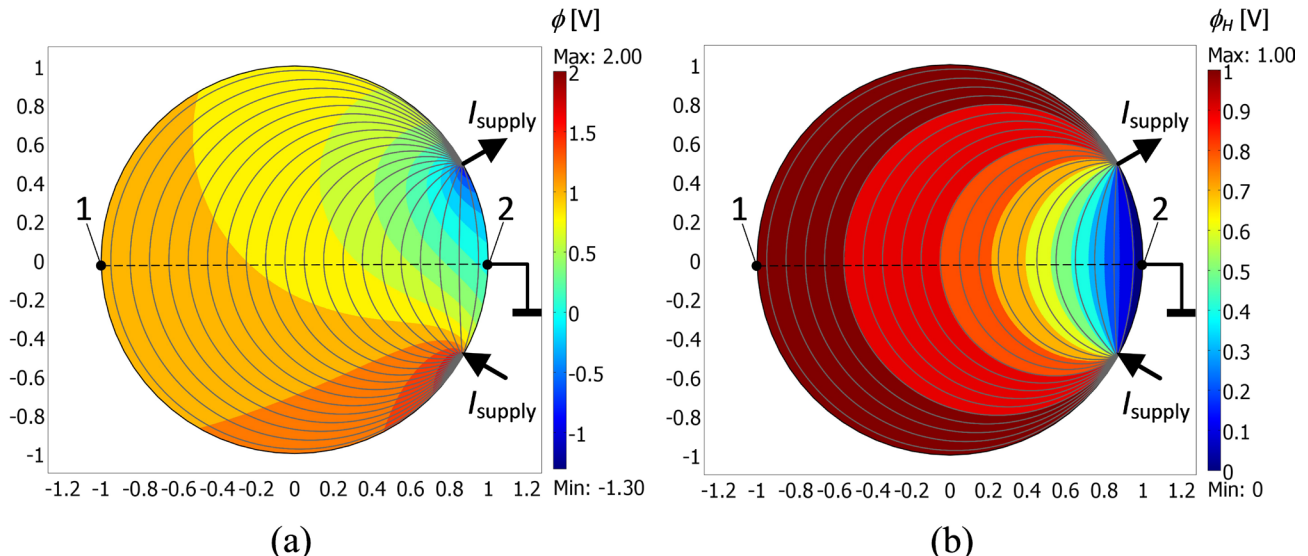


Figure 6. A circular Hall unit disk with point-sized current contacts at azimuthal angles $\pm 30^\circ$. $I_{\text{supply}} = 1\text{A}$, $R_{\text{sheet}} = 1\Omega$, $\mu_H B_{a,z} = 1$. Point 1 is grounded. The integration path in (16) between points 1 and 2 is dashed. (a) Shows the current streamlines in grey color and the electric potential in Volts according to the color map. The potential at the point-sized contacts is finite due to the finite mesh size in the FEM model; (b) Shows current streamlines in grey color and the Hall potential in Volts according to the color map. It shows that the Hall potential is constant on the current streamlines.

7. Hall Plates with One Hole and with Point Current Contacts on the Same Boundary

These are plane domains with the shape of a ring. After Riemann's mapping theorem, *a ring of general shape can always be mapped onto the annular region between two concentric circles* [34] [35]. One radius is arbitrary but the ratio of both radii is fixed by the so-called modulus of the doubly connected region. The modulus is a measure of the size of the hole, and it relates to the resistance between inner and outer boundary at zero magnetic field, if both boundaries are thought to be contacts at different potentials (like in a Corbino disk). We set the outer radius equal to 1 and the inner radius is $0 < r_1 < 1$.

First we assume that all current contacts are on the outer circle as shown in **Figure 7**. At zero applied magnetic field the stream function can be computed analytically as an infinite sum (see **Appendix A**). Since the hole is at a constant value of the stream function, it is encircled by a current streamline and the Hall potential is constant there. The difference of the Hall potential at the hole boundary and at the outer segments agrees with the percentage of current, which is flowing left and right of the hole. The closer the current contacts are together, the more current passes by at this side of the hole. If the contacts are right of the hole as in **Figure 7** and if we ground the right segment of the outer circle (which is at the RHS of the current streamlines), then the Hall geometry factor on the hole boundary approaches 1 as the current contacts approach the ground node in point 1. *The Hall potential of the hole boundary is independent of the size of the hole*: no matter if the central hole is small or large, there is always the same

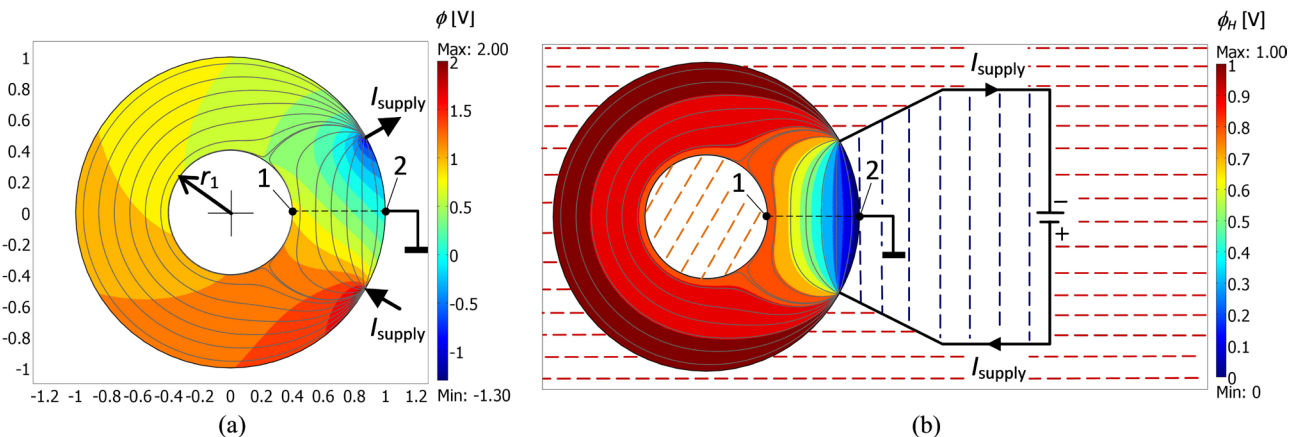


Figure 7. A circular Hall unit disk with insulating hole boundary and with peripheral point-sized current contacts at azimuthal angles $\pm 30^\circ$. $r_1 = 0.4$, $I_{\text{supply}} = 1 \text{ A}$, $R_{\text{sheet}} = 1\Omega$, $\mu_H B_{a,z} = 1$. Point 2 is grounded. The integration path between points 1 and 2 for computing the Hall potential on the hole boundary is the black dashed line. (a) Shows the current streamlines in grey color and the electric potential in Volts according to the color map. The potential at the point-sized contacts is finite due to the finite mesh size in the FEM model; (b) Shows current streamlines in grey color and the Hall potential in Volts according to the color map. It shows that the Hall potential is constant on the current streamlines. Note also two close current streamlines which encircle the hole. The battery and the current return path are also shown outside the sample. The hatched regions inside and outside the current return loop show that H_z is homogeneous there and it equals the values on the boundary (if the geometry extends infinitely in the direction perpendicular to the drawing plane). Also inside the hole H_z is homogeneous and equal to the value on the hole boundary.

current partitioning between left and right, which depends solely on the spacing of contacts (see **Appendix A**).

With the principle of RMFR [23] [24] [25] we can swap supply and sense contacts. Then the Hall potential on the outer boundary is constant if both current contacts are located on the inner boundary. If both current contacts are either on the inner boundary or on the outer boundary and the Hall potential is tapped between two points inside the annulus, its value is readily given by (17a, A5a).

Since the current streamlines do not change with applied magnetic field, we can cut the Hall plate of **Figure 7** along the specific current streamline, which encircles the hole, in two parts without changing the pattern of current flow (see **Figure 8**). The supply currents of both disjunct and simply connected regions are equal to the current partitioning in the original device. The current density fields exactly match before and after cutting. We know that the Hall potential is constant along current streamlines. Therefore it is constant along the cut line and along the hole before and after cutting, because the current streamlines were not changed by the cut. Before the cut we had a single ground node—after the

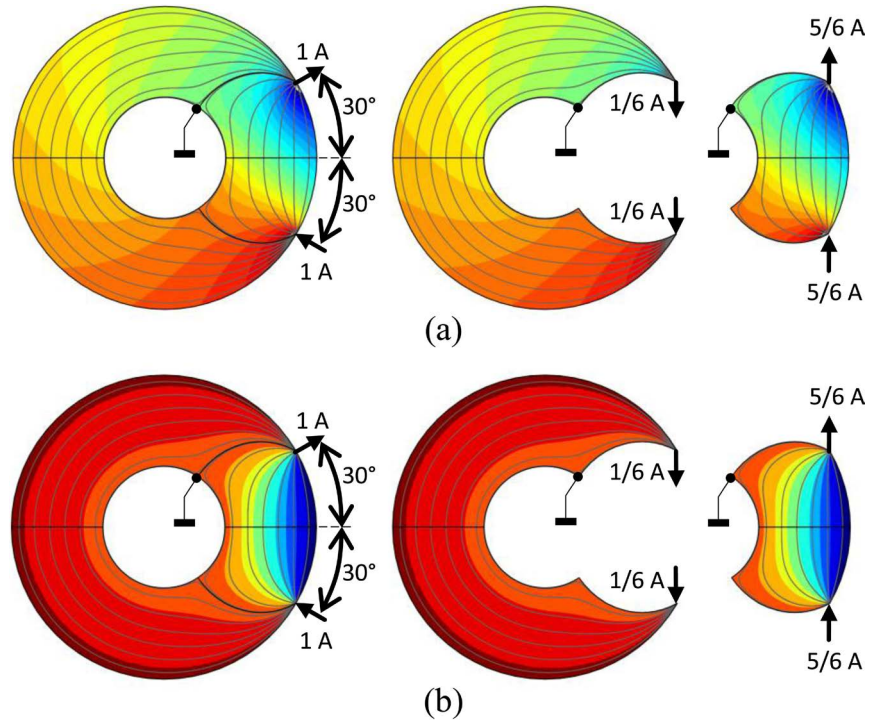


Figure 8. A circular Hall unit disk with insulating hole and with point-sized current contacts at azimuthal angles $\pm 30^\circ$ is split up in its left and right current path around the hole. The current partitioning is 1 to 5 (see also (A6)). The figures show the current streamlines in grey color and the potential at $\mu_H B_{a,z} = 1$ in (a) and the Hall potential in (b) (blue denotes minimum, red is maximum). The current streamlines at arbitrary magnetic field are not disturbed by the cut. The Hall potentials in the split parts are identical to the ones in the complete ring region, because the split parts were grounded in such a way as to establish continuity of the Hall potential like in the original device (see also **Appendix A** for details of analytical computation).

cut we have two disjunct Hall plates and we have to ground both of them. If we ground them along the cut line we re-establish original continuity of Hall potential across the cut line as it was in the original device before cutting. But this means that the two parts of the hole are also tied to the very same Hall potential, which gives zero Hall voltage between two points of the original hole boundary. On the left boundary of the left device the Hall geometry factor is 1 because it is left of the current flow and we grounded the opposite boundary, and on the right boundary of the right device it is -1 because it is right of the current flow and we grounded the opposite boundary. The current through the left device is ζI_{supply} and the current through the right device is $(1-\zeta)I_{\text{supply}}$ with $\zeta=1/6$ denoting the current splitting in [Figure 8](#) ($\alpha=30^\circ=1/6 \times 180^\circ$, cf. [Appendix A](#)). Thus, the Hall voltage between contacts on the original outer boundaries is $V_H = R_{\text{sheet}} \tan \theta_H ((+1)(1-\zeta)I_{\text{supply}} - (-1)\zeta I_{\text{supply}})$, which is identical to the original Hall plate $V_H = R_{\text{sheet}} \tan \theta_H I_{\text{supply}}$ with $G_H=1$. This also solves the riddle of the “anti-Hall bar within a Hall bar” of [Section 2](#).

8. Hall Plates with Several Holes and with Point Current Contacts on the Same Boundary

As long as all current contacts are on boundaries and the net current into each boundary is zero, the problem can be described by a stream function. In the case of point contacts this stream function is constant versus applied magnetic field, as in the previous sections. If several hole boundaries have identical value of the stream function, there is no Hall voltage between them. An example is shown in [Figure 9](#), where we played with the position of the current contacts on the large

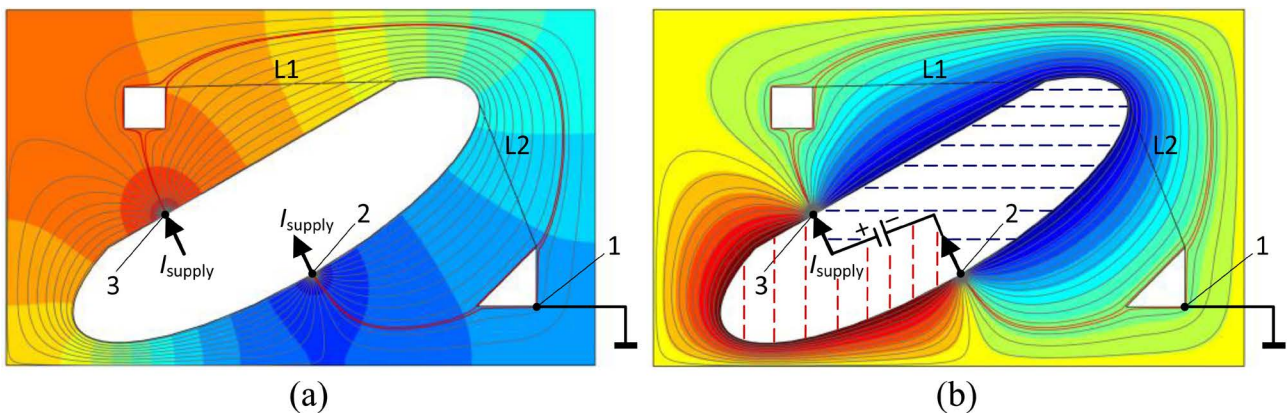


Figure 9. A rectangular Hall plate with three holes with insulating boundaries. Point-sized current contacts are at the boundary of the largest hole. Point 1 is grounded. Two solid straight black lines L1, L2 are the integration paths between small holes and large hole for computing the current through them. (a) Shows the current streamlines in grey color and the electric potential in color map, both at zero magnetic field; (b) Shows current streamlines in grey color and the Hall potential in color map for non-zero magnetic field. The battery and the current return path are also shown inside the large hole. The hatched regions in the large hole show that H_z is homogeneous and the same as on the hole boundary there. The red current flowline encircles both small holes. Thus, there is no Hall voltage between points on the hole boundaries of the square hole and of the triangular hole. All displayed quantities were obtained in an FEM simulation with COMSOL MULTIPHYSICS (Color maps: blue means negative values, red means positive values).

hole boundary until the current through the straight black lines L1, L2 became equal. Thus there is a single streamline (in red color) being split in two parts by the first hole, then joining up again to a single streamline and being split up again in two parts by the second hole. Therefore, the Hall potential is identical on the boundaries of the square and triangular holes. On the outer boundary the Hall potential is also constant but not equal to the one on the hole boundaries.

9. Hall Plates with Extended Contacts at Large Hall Angle

In [Figure 3](#) and [Figure 4](#) we saw that extended contacts tend to behave similar to point sized contacts for large Hall angles. This is explained in [Figure 10](#), where the conductive region covers the upper half plane and current flows from infinity to an extended contact at the bottom in $-1 < x < 1$. At zero applied magnetic field the current enters the contact perpendicularly. However, with increasing magnetic field the current streamlines tilt against the perpendicular direction by the Hall angle. In the limit of 90° Hall angle the current streamlines are forced to flow parallel to the contact—thus, they flow in the same tangential direction as if the contacts were insulating boundaries. Then all current is pushed to the very end of the contact, where we have a current crowding as if it were a point-sized contact. Thereby, the sign of the Hall angle decides if the current is pushed to the left or to the right end of the contact. Near the “active” end of the contact the current density has semi-circular contour lines like with real point-sized contacts.

This behavior can be studied analytically by conformal mapping of the z -plane in [Figure 11\(a\)](#) onto the w -plane in [Figure 11\(b\)](#). In the z -plane the current flows in the upper half plane from infinity ($z = \infty + i\infty$) to the contact between $z = -1 + i \times 0$ and $z = 1 + i \times 0$. This latter contact is grounded: its electric potential is tied to 0 V. With the Schwartz-Christoffel mapping

$$\frac{dw}{dz} = \frac{2i}{\pi} \exp(i\theta_H) \cos \theta_H (z+1)^{\theta_H/\pi-1/2} (z-1)^{-\theta_H/\pi-1/2} \quad (28)$$

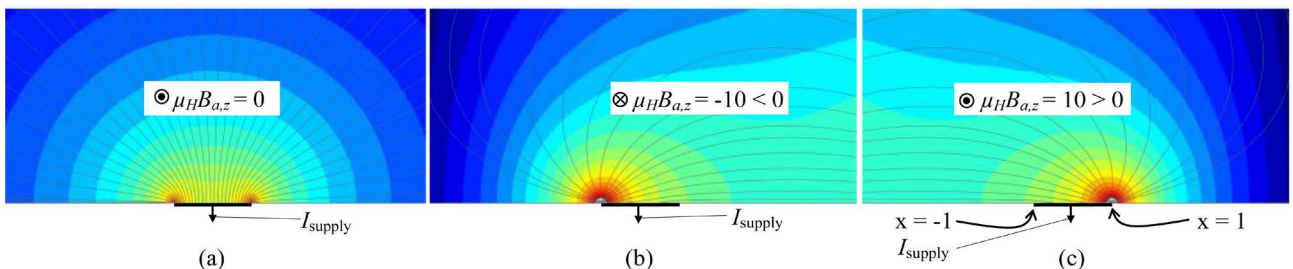


Figure 10. Semi-infinite Hall effect region $y > 0$ with solid black current output contact in the center of the straight lower boundary. The figures show current streamlines in grey color and the magnitude of the current density in color mapping: large values are red, low values near zero are blue, values larger than red are clipped and appear white. The color coding is identical for all three figures. These are results of a 2D FEM simulation with COMSOL MULTIPHYSICS. (a) At zero magnetic field; (b) At $\mu_H B_{a,z} = -10$; (c) At $\mu_H B_{a,z} = 10$. At large Hall angles the current streamlines are nearly parallel to large parts of the elongated contact. The current is squeezed into the left end point of the contact at positive magnetic field and into the right end point of the contact at negative magnetic field. Near the end points the current density has semi-circular contour lines, which is similar to point-sized contacts. Due to the point-like behavior of the contacts the current density is larger at large Hall angles.

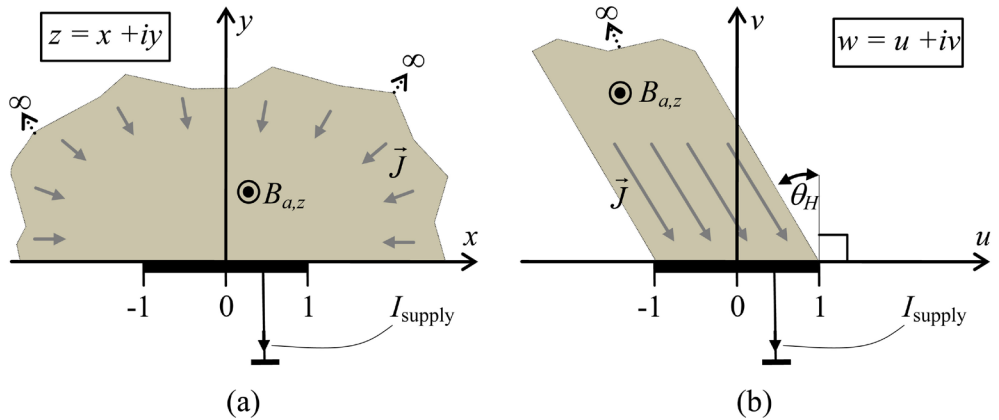


Figure 11. Conformal mapping of the Hall effect region in the upper half z -plane in (a) onto the semi-infinite slanted strip in the w -plane in (b) according to (24). In the w -plane current density, electric field, and electric potential are homogeneous.

the upper half z -plane is mapped onto the strip of infinite length in the w -plane. The strip is slanted by the Hall angle, and the contact is between $w = -1 + i \times 0$ and $w = 1 + i \times 0$. Due to the slanting the electric potential is constant on horizontal lines. This gives a homogeneous electric field in negative v -direction. The current density is homogeneous and parallel to the long sides of the strip. Therefore the complex potential is

$$F_I(w) = I_{\text{supply}} R_{\text{sheet}} \frac{w}{2 \cos^2 \theta_H} \quad (29)$$

It holds $F_I(w) = F_I(z)$ if w and z are linked by (28). With (25) it follows

$$E(z) = i \frac{dF_I}{dz} = i \frac{dF_I}{dw} \frac{dw}{dz} = -I_{\text{supply}} R_{\text{sheet}} \frac{1 + i \tan \theta_H}{\pi} (z+1)^{\theta_H/\pi-1/2} (z-1)^{-\theta_H/\pi-1/2} \quad (30)$$

and finally we get the current density with (26)

$$J(z) = -I_{\text{supply}} \frac{1}{\pi t_H} (z+1)^{\theta_H/\pi-1/2} (z-1)^{-\theta_H/\pi-1/2} \quad (31)$$

For infinite positive applied magnetic field $\theta_H \rightarrow \pi/2$ and $J(z) \rightarrow -I_{\text{supply}} \pi^{-1} t_H^{-1} (z-1)^{-1}$. This is identical to a negative point current source in $z = 1 + i \times 0$. The current density is constant on semi-circles around this point and it points towards $z = 1 + i \times 0$. At infinite negative applied magnetic field $\theta_H \rightarrow -\pi/2$. Then the center of the semi-circles moves to $z = -1 + i \times 0$. The numerical example in **Figure 10(c)** has a Hall angle of 84.3° which means strong but not infinite magnetic field. Therefore the semi-circles are valid only in the neighborhood of the end points of the grounded contact. At larger distance the current streamlines deviate from the pattern given by point sources. There they are accurately given by (31).

10. Discussion

This paper answers the question “Under which circumstances does the Hall voltage—tapped between two contacts on a boundary in a multiply-connected Hall

plate—vanish?”. This question was kindled by the Hall/Anti-Hall bar configurations in [10]. For symmetrical circular ring domains with extended electrodes on perpendicular axes on both boundaries a rigorous solution via conformal mapping has been known since long ago [9]. For the much larger group of asymmetrical, multiply-connected Hall plates the present paper works out a rigorous theory based solely on the classical laws of macroscopic flow of electric current. For the first time the three necessary requirements are identified: 1) a stream function must exist, 2) all boundaries must be insulating, and 3) the current across any contour starting at one sense contact and ending at the other sense contact must vanish. The first requirement means that the net current through all closed boundaries must vanish (e.g., current input and output contacts must be at the boundary of the same hole or they must be both on the outer perimeter). The second requirement means that all contacts are point-sized. The third requirement means that no Hall voltage drops along any current streamline. If the Hall plate has boundaries without current contacts, there is always a current streamline flowing along these boundaries, and therefore the Hall potential on these boundaries has no spatial change.

Acknowledgements

The author gratefully acknowledges the vivid and fruitful discussions with Prof. Dieter Süss of University of Vienna and Dr. William J. Bruno of New Mexico Consortium, Los Alamos, NM.

Conflicts of Interest

The author declares no conflicts of interest regarding the publication of this paper.

References

- [1] Wick, R.F. (1954) Solution of the Field Problem of the Germanium Gyrator. *Journal of Applied Physics*, **25**, 741-756. <https://doi.org/10.1063/1.1721725>
- [2] Versnel, W. (1981) Analysis of Symmetrical Hall Plates with Finite Contacts. *Journal of Applied Physics*, **52**, 4659-4666. <https://doi.org/10.1063/1.329347>
- [3] Ausserlechner, U. (2017) The Signal-to-Noise Ratio and a Hidden Symmetry of Hall Plates. *Solid-State Electronics*, **135**, 14-23. <https://doi.org/10.1016/j.sse.2017.06.007>
- [4] Homencovschi, D. and Bercia, R. (2018) Analytical Solution for the Electric Field in Hall Plates. *Zeitschrift für Angewandte Mathematik und Physik*, **69**, 97. <https://doi.org/10.1007/s00033-018-0989-7>
- [5] Isenberg, I., Russell, B.R. and Greene, R.F. (1948) Improved Method for Measuring Hall Coefficients. *Review of Scientific Instruments*, **19**, 685-688. <https://doi.org/10.1063/1.1741078>
- [6] Rudan, M., et al. (2006) Theory and Experimental Validation of a New Analytical Model for the Position-Dependent Hall Voltage in Devices with Arbitrary Aspect Ratio. *IEEE Transactions on Electron Devices*, **53**, 314-322. <https://doi.org/10.1109/TED.2005.862510>

- [7] Raman, J., Rombouts, P. and Weyten, L. (2013) Method for Electric Field and Potential Calculations in Hall Plates. *Electronics Letters*, **49**, 33-34.
<https://doi.org/10.1049/el.2012.3366>
- [8] Ausserlechner, U. (2016) A Method to Compute the Hall-Geometry Factor at Weak Magnetic Field in Closed Analytical Form. *Electrical Engineering*, **98**, 189-206.
<https://doi.org/10.1007/s00202-015-0351-4>
- [9] Haeusler, J. (1967) Die Untersuchung von Potentialproblemen bei tensorieller Leitfähigkeit der Halbleiter und Plasmen im transversalen Magnetfeld. Dissertation TH Stuttgart. (In German)
- [10] Mani, R.G. and Von Klitzing, K. (1994) Temperature-Insensitive Offset Reduction in a Hall Effect Device. *Applied Physics Letters*, **64**, 3121-3123.
<https://doi.org/10.1063/1.111974>
- [11] Antipov, Y. and Silvestrov, V. (2010) Hilbert Problem for a Multiply Connected Circular Domain and the Analysis of the Hall Effect in a Plate. *Quarterly of Applied Mathematics*, **68**, 563-590. <https://doi.org/10.1090/S0033-569X-2010-01189-1>
- [12] Briane, M. and Milton, G.W. (2009) Homogenization of the Three-Dimensional Hall Effect and Change of Sign of the Hall Coefficient. *Archive for Rational Mechanics and Analysis*, **193**, 715-736. <https://doi.org/10.1007/s00205-008-0200-y>
- [13] Kern, C., Kadic, M. and Wegener, M. (2017) Experimental Evidence for Sign Reversal of the Hall Coefficient in Three-Dimensional Metamaterials. *Physical Review Letters*, **118**, Article ID: 016601. <https://doi.org/10.1103/PhysRevLett.118.016601>
- [14] Bierwagen, O., Ive, T., Van de Walle, C.G. and Speck, J.S. (2008) Causes of Incorrect Carrier-Type Identification in van der Pauw-Hall Measurements. *Applied Physics Letters*, **93**, Article ID: 242108. <https://doi.org/10.1063/1.3052930>
- [15] van Haaren, J.A.M.M. (1988) Macroscopic Current Diversion in Magnetic Fields in Metals and Semiconductors. Doctoral Dissertation, University of Nijmegen, Nijmegen.
- [16] Betz, A. (1964) Konforme Abbildung. 2nd Edition, Chapter IV, Springer Verlag, Berlin. (In German) <https://doi.org/10.1007/978-3-642-87217-4>
- [17] Oszwaldowski, M., Pieranski, P., Berus, T. and Jankowski, J. (2010) Reinterpretation of Hall Effect in Medium with Hole.
- [18] Szymański, K., Cieśliński, J.L. and Łapiński, K. (2013) Van der Pauw Method on a Sample with an Isolated Hole. *Physics Letters A*, **377**, 651-654.
<https://doi.org/10.1016/j.physleta.2013.01.008>
- [19] Oh, D., Ahn, C., Kim, M., Park, E.K. and Kim, Y.S. (2016) Application of the van der Pauw Method for Samples with Holes. *Measurement Science and Technology*, **27**, Article ID: 125001. <https://doi.org/10.1088/0957-0233/27/12/125001>
- [20] Oswald, M., Oswald, J. and Mani, R.G. (2005) Voltage and Current Distribution in a Doubly Connected Two-Dimensional Quantum Hall System. *Physical Review B*, **72**, Article ID: 035334. <https://doi.org/10.1103/PhysRevB.72.035334>
- [21] Kriisa, A., Mani, R.G. and Wegscheider, W. (2010) Hall Effects in Doubly Connected Specimens. *IEEE Transactions on Nanotechnology*, **10**, 179-182.
<https://doi.org/10.1109/TNANO.2010.2049117>
- [22] Popovic, R.S. (2004) Hall Effect Devices, Appendix E. IoP Publishing, Bristol.
<https://doi.org/10.1887/0750308559>
- [23] Spal, R. (1980) A New DC Method of Measuring the Magnetoconductivity Tensor of Anisotropic Crystals. *Journal of Applied Physics*, **51**, 4221-4225.
<https://doi.org/10.1063/1.328281>

- [24] Sample, H.H., Bruno, W.J., Sample, S.B. and Sichel, E.K. (1987) Reverse-Field Reciprocity for Conducting Specimens in Magnetic Fields. *Journal of Applied Physics*, **61**, 1079-1084. <https://doi.org/10.1063/1.338202>
- [25] Cornils, M. and Paul, O. (2008) Reverse-Magnetic-Field Reciprocity in Conductive Samples with Extended Contacts. *Journal of Applied Physics*, **104**, Article ID: 024505. <https://doi.org/10.1063/1.2951895>
- [26] Munter, P.J.A. (1990) A Low-Offset Spinning Current Hall Plate. *Sensors Actuat A*, **21-23**, 743-746. [https://doi.org/10.1016/0924-4247\(89\)80069-X](https://doi.org/10.1016/0924-4247(89)80069-X)
- [27] Ausserlechner, U. (2004) Limits of Offset Cancellation by the Principle of Spinning Current Hall Probe. *Proceedings of IEEE SENSORS*, Vienna, 24-27 October 2004, 1117-1120. <https://doi.org/10.1109/ICSENS.2004.1426372>
- [28] Madec, M., Kammerer, J.B., Hébrard, L. and Lallement, C. (2011) Analysis of the Efficiency of Spinning-Current Techniques Thru Compact Modeling. *Sensors*, Limerick, 28-31 October 2011, 542-545. <https://doi.org/10.1109/ICSENS.2011.6127318>
- [29] Motz, M., Ausserlechner, U., Scherr, W. and Katzmaier, E. (2006) An Integrated Hall Sensor Platform Design for Position, Angle and Current Sensing. *Sensors*, Daegu, 22-25 October 2006, 1008-1011. <https://doi.org/10.1109/ICSENS.2007.355795>
- [30] Buehler, M.G. and Pearson, G.L. (1966) Magnetoconductive Correction Factors for an Isotropic Hall Plate with Point Sources. *Solid-State Electronics*, **9**, 395-407. [https://doi.org/10.1016/0038-1101\(66\)90154-7](https://doi.org/10.1016/0038-1101(66)90154-7)
- [31] Schott, C., Randjelovic, Z., Waser, J.M. and Popovic, R.S. (1998) 2D Nonlinearity Simulation of the Vertical Hall Sensor Using SESES. *1st International Conference on Modeling and Simulation of Microsystems, Semiconductors, Sensors and Actuators*, Santa Clara, 6-8 April 1998, 643-648.
- [32] Weissman, M.B. (1980) Relations between Geometrical Factors for Noise Magnitudes in Resistors. *Journal of Applied Physics*, **51**, 5872-5875. <https://doi.org/10.1063/1.327550>
- [33] Kern, C., Milton, G.W., Kadic, M. and Wegener, M. (2018) Theory of the Hall Effect in Three-Dimensional Metamaterials. *New Journal of Physics*, **20**, Article ID: 083034. <https://doi.org/10.1088/1367-2630/aad92b>
- [34] Schinzinger, R. and Laura, P.A.A. (2003) Conformal Mapping. Dover Publications Inc., Mineola.
- [35] Komatu, Y. (1949) Existence Theorem of Conformal Mapping of Doubly-Connected Domains. *Kodai Mathematical Seminar Reports*, **1**, 3-4. <https://doi.org/10.2996/kmj/1138833531>
- [36] Stafl, M. (1967) Electrodynamics of Electrical Machines. Academia, Publishing House of the Czechoslovak Academy of Sciences, Praha, Chapter 2.6.
- [37] Schuh, F. (1919) Theorem on the Term by Term Differentiability of a Series. *KNAW Proceedings*, 22 I, 1919-1920, Amsterdam, 376-378.

Appendix A

Here we compute the current pattern for the Hall plate with insulating hole boundary and point-sized supply contacts at the outer boundary (see [Figure 7](#)). In principle one can do the calculation with the potential ϕ or with the stream function ψ . However, with the potential one encounters the following problem: If we make a Fourier separation ansatz for ϕ we need to fulfill the conditions for the radial current density $J_r = \partial\phi/\partial r$ at the insulating boundaries. Thereby, we have to differentiate the series term wise, which reduces the convergence of the series drastically—it even diverges at $r=1$. Whenever we do not manage to find a closed formula for the sum of the ϕ -series we should avoid boundary conditions that use derivatives of ϕ . Conversely, for the stream function we do not need derivatives at the insulating boundary, which facilitates the calculation.

We use polar coordinates (r, φ) . The current input contact is located in $r=1, \varphi=-\alpha$, the current output is in $r=1, \varphi=\alpha$ with $0 < \alpha < \pi$. The annular conductive region is in $r_i \leq r \leq 1$ with $0 < r_i < 1$. For the stream function ψ we make the ansatz (see [36])

$$\psi = (A_0 \ln r + B_0)(C_0 \varphi + 1) + \sum_{k=1}^{\infty} (A_k r^k + B_k r^{-k})(C_k \sin k\varphi + \cos k\varphi). \quad (\text{A1})$$

From periodicity requirement $\psi(r, \varphi) = \psi(r, \varphi + 2\pi) \forall r$ it follows $C_0 = 0$. The outer boundary is split up in a left segment $\varphi \in (-\pi, -\alpha) \cup (\alpha, \pi)$ and a right segment $\varphi \in (-\alpha, \alpha)$. In both segments the stream function has to be constant according to (18), because no current flows through the boundary. According to our rule (see (16c)) we set its value at the grounded segment to zero: $\psi_{\text{right}} = 0$. At the left segment its value is ψ_{left} . With (18) we get

$$-\frac{\psi_{\text{right}} - \psi_{\text{left}}}{R_{\text{sheet}}} = \lim_{\varepsilon \rightarrow 0} t_H \mathbf{n}_z \cdot \int_{\varphi=-\alpha-\varepsilon}^{-\alpha+\varepsilon} \frac{-I_{\text{supply}}}{2\varepsilon t_H} \mathbf{n}_r \times \mathbf{n}_{\varphi} d\varphi = -I_{\text{supply}}. \quad (\text{A2})$$

\mathbf{n}_r and \mathbf{n}_{φ} are the unit vectors in radial and azimuthal directions, respectively. On the inner insulating boundary without current contacts it has some constant value $\psi = \psi_{\text{hole}} \forall \varphi$, which leads to $B_k = -A_k r_i^{2k} \forall k \geq 1$. Thus, ψ is given on all boundaries (Dirichlet problem) and it is an even function in φ . Therefore $C_k = 0 \forall k \geq 1$.

With $\nabla \cdot \mathbf{E} = 0$ it follows from Gauss' theorem $\int_{\varphi=-\pi}^{\pi} \partial\phi/\partial r r d\varphi = 0$ for $r_i < r < 1$. With (16c) it follows at arbitrary applied magnetic field:

$\int_{\varphi=-\pi}^{\pi} \partial\psi/\partial r r d\varphi = 0$. With (A1) this gives $A_0 = 0$. Thereby it is allowed to differentiate the ansatz (A1) term-wise because with A_k obtained below in (A4b) the term-wise differentiated series converges uniformly in $r_i < r < 1$ [37].

B_0 is obtained from computing the mean of ψ on the outer perimeter

$$\int_{\varphi=-\pi}^{\pi} \psi(r=1) d\varphi = 2\pi B_0 = 2(\pi - \alpha)\psi_{\text{left}} = -2(\pi - \alpha)I_{\text{supply}}R_{\text{sheet}}. \quad (\text{A3})$$

and A_k is obtained by the Fourier series expansion of ψ on the outer perimeter

$$\begin{aligned} \int_{\varphi=-\pi}^{\pi} \psi(r=1) \cos k\varphi d\varphi &= \int_{\varphi=-\pi}^{\pi} (1 - r_1^{2k}) A_k \cos^2 k\varphi d\varphi \\ &= \int_{\varphi=-\pi}^{-\alpha} + \int_{\varphi=\alpha}^{\pi} (-1) I_{\text{supply}} R_{\text{sheet}} \cos k\varphi d\varphi \end{aligned} \quad (\text{A4a})$$

$$\Rightarrow A_k = I_{\text{supply}} R_{\text{sheet}} \frac{\alpha}{\pi} \frac{\sin k\alpha}{k\alpha} \frac{2}{1 - r_1^{2k}}. \quad (\text{A4b})$$

Finally, the stream function (with and without applied magnetic field) is given by

$$\psi = I_{\text{supply}} R_{\text{sheet}} \left[\frac{\alpha}{\pi} \left(1 + 2 \sum_{k=1}^{\infty} \frac{r^k - r_1^{2k} r^{-k}}{1 - r_1^{2k}} \frac{\sin k\alpha}{k\alpha} \cos k\varphi \right) - 1 \right]. \quad (\text{A5a})$$

The series can be summed up if the hole vanishes

$$\psi|_{r_1=0} = I_{\text{supply}} R_{\text{sheet}} \frac{1}{\pi} \left(\alpha - \pi + \arctan \frac{r \sin(\alpha - \varphi)}{1 - r \cos(\alpha - \varphi)} + \arctan \frac{r \sin(\alpha + \varphi)}{1 - r \cos(\alpha + \varphi)} \right). \quad (\text{A5b})$$

The stream function is finite everywhere, and it is continuous except in the current contacts where it jumps only along the boundary. Now we compute the current that flows at the RHS of the hole. The current density on the x-axis is $\mathbf{J} = \rho^{-1} \partial \psi / \partial r \mathbf{n}_\varphi$. With (18) and [Figure 7](#) we get

$$I_{12} = t_H \mathbf{n}_z \cdot \int_1^2 \mathbf{J} \times d\mathbf{s} = t_H \mathbf{n}_z \cdot \int_{x=r_1}^{x=1} J_y \mathbf{n}_y \times \mathbf{n}_x dx = -t_H \int_{x=r_1}^{x=1} J_y dx = -I_{\text{supply}} \left(1 - \frac{\alpha}{\pi} \right). \quad (\text{A6})$$

Point 2 is the ground node in $(r, \varphi) = (1, 0)$ and point 1 is on the hole boundary in $(r, \varphi) = (r_1, 0)$. We used the sum $\sum_1^{\infty} k^{-1} \sin \alpha k = (\pi - \alpha)/2$ for $0 < \alpha \leq \pi$. With (19) the Hall geometry factor for one probe on the hole boundary against grounded point 2 is

$$G_{H,12} = 1 - \alpha/\pi \quad (\text{A7})$$

Thus, the Hall geometry factor on the hole boundary is 1 for $\alpha \rightarrow 0^\circ$, 0.5 for $\alpha = 90^\circ$, and 0 for $\alpha \rightarrow 180^\circ$. This symmetry agrees with common sense. Interestingly, the current I_{12} at the RHS of the hole is independent on the size of the hole r_1 . This also holds for the Hall voltage measured between a point on the hole and a point on the outer boundary.

On the hole boundary the sum in (A5a) vanishes and we get

$$\psi(r = r_1, \varphi = 0) = \psi_{\text{hole}} = I_{\text{supply}} R_{\text{sheet}} \left(\frac{\alpha}{\pi} - 1 \right). \quad (\text{A8})$$

On the right segment of the outer boundary we have in accordance with (A2)

$$\psi(r = 1, |\varphi| < \alpha) = \psi_{\text{right}} = 0 \quad (\text{A9a})$$

and on the left segment of the outer boundary we have

$$\psi(r = 1, \varphi \notin [-\alpha, \alpha]) = \psi_{\text{left}} = -I_{\text{supply}} R_{\text{sheet}}. \quad (\text{A9b})$$

The Hall geometry factor between points on left and right segment of the outer boundary is simply 1, independent of the hole and its size.

We call the path along which the specific current streamline flows, which separates the annulus into left and right branches of current flow around the hole, the *separation curve*. It meets the inner circle at a right angle and it meets the outer circle in the current contact at the angle α . This is obvious if we note that the current flows isotropically out of the current contact (which is proven below) and the fraction α/π takes the left detour around the hole. If we want to compute the separation curve, we have to solve $\psi(r, \varphi) = \psi_{\text{hole}}$ which gives

$$\sum_{k=1}^{\infty} \frac{r^k - r_1^{2k} r^{-k}}{1 - r_1^{2k}} \frac{\sin k\alpha}{k} \cos k\varphi = 0. \quad (\text{A10})$$

We used this in [Figure 8](#) where we computed 16 uniformly spaced points on the separation curve by solving (A10) numerically and input the curve into the geometry model of an FEM simulation. Then we cut the ring along this separation curve into two simply connected regions. A fine mesh of 3 million elements was made. The resulting currents through the straight horizontal lines in the circular ring matched up to 0.3 ppm with the currents through the simply connected devices in the center and at the RHS of [Figure 8](#). The Hall voltage was computed between left and right points on the boundary in $y = 0$ for a strong magnetic field with 45° Hall angle. It matched up to 2 ppm for simply and doubly connected regions.

With ψ we know the Hall potential ϕ_H according to (17a), but not the potential $\phi = \phi_0 + \phi_H$. The potential at zero applied magnetic field is obtained by integrating the Cauchy-Riemann differential equations (20a, b).

$$\phi_0 = \frac{\partial}{\partial \varphi} \int \frac{\psi}{r} dr = I_{\text{supply}} R_{\text{sheet}} \frac{-2\alpha}{\pi} \sum_{k=1}^{\infty} \frac{r^k + r_1^{2k} r^{-k}}{1 - r_1^{2k}} \frac{\sin k\alpha}{k\alpha} \sin k\varphi. \quad (\text{A11a})$$

ϕ_0 is finite except in the current contacts. It is zero on the x-axis and odd in φ and α . If the ring degenerates to a disk $r_1 \rightarrow 0$ we can sum it up in terms of elementary functions

$$\phi_0|_{r_1=0} = I_{\text{supply}} R_{\text{sheet}} \frac{1}{2\pi} \ln \frac{1+r^2 - 2r \cos(\varphi - \alpha)}{1+r^2 - 2r \cos(\varphi + \alpha)}. \quad (\text{A11b})$$

For $r_1 \rightarrow 0$ the streamline $\psi = \omega I_{\text{supply}} R_{\text{sheet}}$ with $-1 \leq \omega \leq 0$ is a circle with radius $|\sin \alpha| / |\sin(\alpha + \omega\pi)|$ having its center at $x = \sin \omega\pi / \sin(\alpha + \omega\pi)$ and $y = 0$. This can be shown by entering the points on this circle into (A5b), eliminating y , and differentiating w.r.t. x , which gives zero. Hence, along this circle the stream function is constant. The circular stream function crosses the x-axis in $x = \cos(-\alpha/2 + \omega\pi/2) / \cos(\alpha/2 + \omega\pi/2)$.

We draw a small circle of radius $\delta r \rightarrow 0$ around the negative current contact in $\mathbf{r}^{(-)} = (\cos \alpha, \sin \alpha)$. At points within this circle we compute the current density with (A5b) and (13). A series of the current density in powers of δr has the dominant term $\mathbf{J} = -I_{\text{supply}} (\mathbf{r} - \mathbf{r}^{(-)}) / \left(\pi t_H |\mathbf{r} - \mathbf{r}^{(-)}|^2 \right) + O(|\mathbf{r} - \mathbf{r}^{(-)}|^0)$. This proves that the current flows isotropically into the negative supply contact. If two current streamlines are given by $\psi_1 = \omega_1 I_{\text{supply}} R_{\text{sheet}}$ and $\psi_2 = \omega_2 I_{\text{supply}} R_{\text{sheet}}$

a current $|\omega_1 - \omega_2|I_{\text{supply}}$ flows between them according to (18), and in the current contact the two streamlines define an aperture angle of $|\omega_1 - \omega_2|\pi$.

A first streamline $\psi = (-1 + \alpha/\pi)I_{\text{supply}}R_{\text{sheet}}$ goes through the origin (compare with (A5b)). Then it holds $\omega = -1 + \alpha/\pi$ and the radius of this circle is equal to $1/(2\cos\alpha)$. A second streamline is for $\omega = -\alpha/\pi$ which has infinite radius. This is a vertical line through the current contacts. Comparison of first and second streamlines says that the current flowing left of the center is equal to the current flowing right of the current contacts.

The complex potential in the disk without hole can be computed more elegantly without recurring to series developments. Thereby one writes down the current density \mathbf{J} in the upper half plane when a current enters the half plane in $x = -1$: $\mathbf{J} = I_{\text{supply}}\pi^{-1}t_H^{-1}((x+1)\mathbf{n}_x + y\mathbf{n}_y)/((x+1)^2 + y^2)$. Thus, the potential at zero magnetic field is $\phi_0 = -\rho I_{\text{supply}}\pi^{-1}t_H^{-1}\ln\sqrt{(x+1)^2 + y^2}$. Then the complex potential is obtained as the analytic function whose real part is ϕ_0 . This gives $\phi_0 + i\psi = -\rho I_{\text{supply}}\pi^{-1}t_H^{-1}\ln(z+1)$ with $z = x + iy$. With the mapping $z = -i \cot(\alpha/2)(w-1)/(w+1)$ the upper half of the z -plane is mapped inside the unit disk in the w -plane with the current input at $w = \exp(-i\alpha)$. Subtracting the contribution of the outgoing current at $x = 1$ one gets the complex potential at zero magnetic field

$$\phi_0 + i\psi = \frac{I_{\text{supply}}R_{\text{sheet}}}{\pi} \left(\ln\left(\frac{-i}{\tan(\alpha/2)} \frac{z-1}{z+1} - 1\right) - \ln\left(\frac{-i}{\tan(\alpha/2)} \frac{z-1}{z+1} + 1\right) \right) \quad (\text{A12})$$

which matches (A5b, A11b).